Mechanism and Kinetics of δ-Lysin Interaction with Phospholipid Vesicles†

Antje Pokorny,‡ T. Harry Birkbeck,§ and Paulo F. F. Almeida*,‡

Department of Chemistry, University of North Carolina at Wilmington, Wilmington, North Carolina 28403, and Institute of Biomedical and Life Sciences, Division of Infection and Immunity, Joseph Black Building, University of Glasgow, Glasgow G12 8QQ, Scotland

Received March 27, 2002; Revised Manuscript Received July 9, 2002

ABSTRACT: δ-Lysin is a 26 amino acid, hemolytic peptide toxin secreted by *Staphylococcus aureus*. It has been reported to form an amphipathic helix upon binding to lipid bilayers and is often cited as a typical example of the barrel-stave model for pore formation in lipid bilayer membranes. However, the exact mechanism by which it lyses cells and the physical basis of its target specificity are still unknown. Moreover, the evidence for δ-lysin insertion and pore formation in the membrane stems largely from theoretical modeling of the toxin and lacks experimental confirmation. We investigated binding and insertion of δ-lysin into phospholipid bilayer vesicles. The kinetics of these processes were studied by stopped-flow fluorescence with two types of experiments: (a) carboxyfluorescein release from the vesicles upon peptide−vesicle interaction, with concomitant relief of dye self-quenching; (b) fluorescence energy transfer from the intrinsic tryptophan of the peptide to a membrane-bound lipid probe. We formulated a detailed kinetic mechanism with explicit molecular rate constants for peptide binding, association, and insertion, obtaining a quantitative description of the experimental results. δ-Lysin insertion is strongly dependent on the peptide-to-lipid ratio, suggesting that association of a critical number of monomers on the membrane is required for activity. However, we found no evidence for a stable membrane-inserted pore. Rather, the peptide appears to cross the membrane rapidly and reversibly and cause release of the lipid vesicle contents in this process.

Many unrelated organisms produce short, linear, cytolytic peptides, usually between 15 and 30 amino acids in length, that play a role in the defense against competing or attacking organisms (for recent reviews see refs *1*−*4*). In eukaryotes, they appear to be a component of a nonadaptive immune system that protects the host organism against invading microorganisms. As a consequence, they are often found on body surfaces, such as skin and intestines, or in the blood and hemolymph (*5*). These peptides have received much attention in recent years because they could represent an alternative to classical antibiotics, given their preferential lysis of bacteria and fungi (*6*). Exactly how they distinguish between cell types is still under investigation, but it seems relatively certain that no cell-surface receptors are involved in the recognition mechanism because synthetic peptides with all-D-amino acid enantiomers show the same activity as the natural, all-L-amino acid peptides (*7*). Thus, some kind of molecular recognition mechanism appears to reside at the level of the lipid bilayer, even though the ultimate target site may be a cellular structure other than the plasma membrane (*8*). Cytolytic peptides are also constituents of the venoms secreted by wasps and bees. Peptides in this category, such as melittin and mastoparan, do not discriminate between cell types (*9*, *10*) but rather lyse cells and model membrane vesicles alike, independent of composition, as if peptides intended for secretion need not distinguish self from nonself, because the target is remote from the source organism. The occurrence of toxic peptides is, however, not restricted to eukaryotic organisms. *Staphylococcus aureus*, a Gram-positive bacterium, also secretes cytolytic peptides as part of a broadly toxic cocktail. Staphylococcal δ-lysin, a 26 amino acid peptide (formyl-NH-Met-Ala-Gln-Asp-Ile-Ile-Ser-Thr-Ile-Gly-Asp-Leu-Val-Lys-Trp-Ile-Ile-Asp-Thr-Val-Asn-Lys-Phe-Thr-Lys-Lys-COO^-), is an interesting example of a rarer subclass of peptides, which lyse eukaryotic cells in preference to bacterial cells in vivo (*11*, *12*).

In general, the amino acid sequences of cytolytic peptides from different organisms vary widely, but many are able to form an amphipathic α-helix. The distribution of charged amino acids along the helix axis varies among these cytotoxic peptides, but most frequently they carry a positive net charge at neutral pH. δ-Lysin is exceptional in this respect: with four basic and three acidic residues, a negative C-terminus, and a formylated N-terminus, it has zero net charge at neutral pH, which facilitates its aggregation in aqueous solution (*13*−*16*). In fact, δ-lysin is soluble in both aqueous and organic solvents such as chloroform/methanol (*13*). A net positive charge is often thought to be required for binding to negatively charged bacterial membranes. The absence of a net charge and lack of activity against many intact bacterial cells in the case of δ-lysin seem to corroborate this idea (*6*, *17*, *18*). However, the antibacterial peptide magainin has been

† This work was supported in part by Grants praxis/p/bio/12015/1998 and praxis/pcna/p/bio/73/96 from the Fundação para a Ciência e Tecnologia (Portugal) and by Grant ERBFMRXCT96004 from the TMR program (EU).

* To whom correspondence should be addressed. Tel: (910) 962-7300. Fax: (910) 962-3013. E-mail: almeidap@uncw.edu.

‡ University of North Carolina at Wilmington.

§ University of Glasgow.

10.1021/bi020244r CCC: $22.00
Published on Web 08/15/2002

shown by isothermal titration calorimetry (*19*) to bind to neutral membranes with association enthalpies similar to those found for charged membranes (*20*), and δ-lysin is able to penetrate both charged and neutral membranes in vitro (*21*). Moreover, positively charged melittin lyses erythrocytes as well as bacterial cells (*1*). Thus, the positive charge of peptides belonging to the innate immune system cannot be the sole cause for their specificity, and other factors may have to be considered, such as the distribution of charge along the peptide axis (*22*). In the case of δ-lysin, the absence of a net charge with the consequent propensity for aggregation in water may simply be a protective measure, perhaps against proteases, rather than a factor in the determination of target cell specificity. In view of these observations, target membrane specificity may be more diverse than generally assumed, and additional mechanisms will have to be taken into account. In this regard, the study of a neutral peptide, such as δ-lysin, targeted at neutral membranes provides insight into a mechanism in which peptide charge is not the major factor. δ-Lysin is believed to bind to the membrane and eventually insert into the hydrophobic bilayer core to form a stable, water-filled, multipeptide pore (*23*−*27*). However, the evidence for this mechanism stems mainly from the observation that δ-lysin forms voltage-dependent channels in artificial phospholipid bilayers (*24*), which were modeled as hexameric channels (*26*). That same study (*24*), however, also reports complex channel opening kinetics and a variety of intermediate conductances which could not be easily accounted for by a stoichiometric pore mechanism.

To understand the mechanism of δ-lysin activity, we conducted a detailed and quantitative investigation of the kinetics of interaction of δ-lysin with phospholipid bilayer vesicles. We found that δ-lysin inserts into the bilayer but does not form a stable pore. Rather, the residence time of the membrane-inserted species is very short, and the peptide translocates across the bilayer in a process that requires prior aggregation on the membrane surface. Translocation, therefore, depends critically on the concentration of δ-lysin on the membrane. At sufficiently high concentrations, the peptide will eventually equilibrate over the outer and the inner membrane surfaces.

MATERIALS AND METHODS

Chemicals. POPC[1] (1-palmitoyl-2-oleoyl-*sn*-glycero-3-phosphocholine) was purchased in chloroform solution form Avanti Polar Lipids, Inc. U6 [4-[(*N*,*N*-dimethyl-*N*-tetradecylammonium)methyl]-7-hydroxycoumarin chloride] was obtained from Molecular Probes Europe, B.V. Chloroform p.A. was from Merck, carboxyfluorescein was from Fluka (Sigma-Aldrich Group, Spain), and all other chemicals were from Sigma Chemical Co. (Sigma-Aldrich Group, Spain). Lipids and other chemicals were used without further purification.

Preparation of Large Unilamellar Vesicles (LUV). POPC solutions in chloroform were placed in a round-bottomed flask, and the solvent was rapidly evaporated using a rotary evaporator (Büchi R-114A) at 60 °C. The lipid film was then placed under vacuum for 3−5 h and hydrated by the addition of buffer to give a final lipid concentration of 10 mM. Swirling of the flask yielded a turbid suspension of multilamellar vesicles, which was subsequently extruded about 10 times through two stacked Nuclepore polycarbonate filters of 0.1 μm pore size. Extrusion was performed with a water-jacketed high-pressure extruder from Lipex Biomembranes Inc. The suspension was diluted in buffer to the desired concentration and used for fluorescence measurements. The buffer used was 20 mM MOPS, pH 7.5, 80 mM KCl, 0.01 mM EGTA, and 0.02% NaN_3. For experiments using carboxyfluorescein encapsulated in POPC vesicles, the lipid film was hydrated in 50 mM carboxyfluorescein, 20 mM MOPS, pH 7.5, 0.01 mM EGTA, and 0.02% NaN_3. Following extrusion, carboxyfluorescein-containing LUVs were passed through a Sephadex G-25 column to separate carboxyfluorescein in the external buffer from the vesicles. Lipid concentrations were assayed using a modified version of the Bartlett phosphate assay (*28*). In short, appropriate volumes of samples and standards were pipetted and adjusted to 300 μL with distilled water. After addition of 700 μL of 70% $HClO_4$, all tubes were covered with glass marbles and placed in a block heater at 200 °C for 30 min or until clear. After cooling, 2 mL of a 1% solution of ammonium molybdate was added to the tubes, followed by 2 mL of a 4% solution of ascorbic acid. The tubes were immediately placed in a water bath for 1 h at 37 °C, and the absorbance was read at 700 nm.

Preparation of δ-Lysin. δ-Lysin was prepared as previously described (*29*). Briefly, *S. aureus* strain NCTC 10345 was grown for 18 h on a rotary shaker at 37 °C in 2 L Erlenmeyer flasks containing 500 mL of yeast extract diffusate medium (*30*). After centrifugation to remove bacterial cells, δ-lysin was removed from the supernatant fluid by adsorption to hydroxylapatite mixed into the supernatant. The hydroxylapatite was washed with 0.001 and 0.4 M phosphate buffers, pH 6.8, before elution of the δ-lysin with 1.0 M phosphate buffer, pH 7.4. After dialysis against distilled water the δ-lysin solution was mixed with an equal volume of 1.0 M trichloroacetic acid at 0 °C to remove any material reacting in the Limulus Amoebocyte Lysate test for endotoxins. The precipitate was collected by centrifugation, dissolved in distilled water, and dialyzed thoroughly against distilled water before lyophilization to yield a white powder. The purity of the peptide was determined as previously described (*29*). Assignment of frequencies and structure determination by NMR indicated an α-helical conformation in methanol and no contaminants (*31*).

Fluorescence Experiments. Steady-state fluorescence measurements were performed in a SLM-Aminco 4800C spectrofluorometer. Kinetic traces were obtained using a Hi-Tech SF-61 stopped-flow fluorometer. For fluorescence energy transfer experiments, U6 was either added externally to the vesicles from a 0.50 mM stock solution in ethanol to a final concentration of 2% of the total lipid (4% U6 in the outer leaflet) or codissolved with the POPC solution at a final concentration of 4% of the total lipid, dried, and extruded as described above. Samples were excited at 295 nm, and the degree of fluorescence energy transfer was measured by collecting the emission from U6 through a GG455 long-pass filter (Schott, Germany). Carboxyfluorescein efflux was

[1] Abbreviations: POPC, 1-palmitoyl-2-oleoyl-*sn*-glycero-3-phosphocholine; PE, phosphatidylethanolamine; U6, 4-[(*N*,*N*-dimethyl-*N*-tetradecylammonium)methyl]-7-hydroxycoumarin chloride; LUV, large unilamellar vesicles; NMR, nuclear magnetic resonance; P/L, peptide-to-lipid ratio.

measured by the relief of self-quenching of fluorescence, measured by excitation at 492 nm and collecting emission through a OG530 long-pass filter (Schott, Germany). For the stopped-flow fluorescence measurements, lyophilized δ-lysin was dissolved in distilled water acidified to pH $\simeq$3 to a final concentration of 200 μM and stored frozen in 50 μL aliquots in Eppendorf tubes. Prior to use, an aliquot was thawed and kept on ice. Immediately before an experiment, 5 μL of this solution was added to 1 mL of 0.10 M KCl, pH 3.0, to avoid changes in the concentration of δ-lysin in solution due to its tendency to stick to glass surfaces. All experiments were done at 22 °C.

In the kinetic analysis of carboxyfluorescein efflux it is important to know at what carboxyfluorescein concentration the dye ceases to be self-quenched. If partially empty vesicles contributed to the fluorescence at later times, that must be included in the analysis of the kinetic traces. To evaluate this contribution, carboxyfluorescein fluorescence was measured as a function of encapsulated dye concentration from 1 μM to 50 mM in POPC vesicles. We found that carboxyfluorescein self-quenching is essentially abolished only at concentrations <0.3 mM and that the total carboxyfluorescein fluorescence varies linearly with the concentration of dye outside the vesicles. Furthermore, we measured the rate of efflux from vesicles containing different amounts of encapsulated carboxyfluorescein, from 1 μM to 50 mM. The kinetics of carboxyfluorescein efflux were independent of the encapsulated dye concentration (data not shown). A correction of the fluorescent traces is thus irrelevant.

Model and Data Analysis. The experimental kinetic data were analyzed with the following model. For the dissociation in aqueous solution:

$$T_w \rightleftharpoons D_w \rightleftharpoons M_w \tag{1}$$

where T_w, D_w, and M_w are solution δ-lysin tetramers, dimers, and monomers, respectively. For binding to and dissociation from the vesicles:

$$M_w + L \rightleftharpoons M_o \tag{2}$$

$$D_w + L \rightleftharpoons D'_o \tag{3}$$

where L represents a lipid vesicle and M_o and D'_o represent monomers and dimers bound to the outer leaflet of the membrane. For the membrane-associated processes:

$$D'_o \rightleftharpoons M_o \rightleftharpoons D_o \quad \text{(outer leaflet)} \tag{4}$$

$$M_o + D_o \rightleftharpoons T_{ins} \rightleftharpoons D_i + M_i \quad \text{(translocation)} \tag{5}$$

$$M_i \rightleftharpoons D_i \quad \text{(inner leaflet)} \tag{6}$$

where D_o is a stable, membrane-associated dimer, which is different from the D'_o dimer, and T_{ins} is a trimer inserted in the lipid bilayer, which is the species responsible for dye efflux. In all equations, species subscripts o or i refer to the outer or inner leaflets of the lipid bilayer, and subscripts w refer to aqueous species. Formation of D'_i dimers and desorption from the inner leaflet into the vesicle interior were not included in the scheme because of the comparatively small magnitudes of the corresponding rate constants (see Results).

These equilibria were written in terms of a set of coupled, nonlinear differential equations, which constitute the kinetic model. Note that all constants referring to solution processes are marked with an asterisk (e.g., k^*_{a1}), whereas constants without an asterisk refer to processes on the membrane or association with the membrane. Refer to Figure 5 for a complete scheme of the model. For δ-lysin addition to dye-containing POPC LUVs, we have

solution species

$$\frac{dT_w}{dt} = -k^*_{d1}T_w + k^*_{a1}{D_w}^2 \tag{7}$$

$$\frac{dD_w}{dt} = 2k^*_{d1}T_w - 2k^*_{a1}{D_w}^2 - k^*_{d2}D_w + k^*_{a2}{M_w}^2 - k_{on2}LD_w + k_{off2}D'_o \tag{8}$$

$$\frac{dM_w}{dt} = 2k^*_{d2}D_w - 2k^*_{a2}{M_w}^2 - k_{on1}LM_w + k_{off1}M_o \tag{9}$$

outer leaflet species

$$\frac{dD'_o}{dt} = k_{on2}LD_w - (k_{off2} + k_{d0})D'_o + k_{a0}{M_o}^2/(\upsilon_o L) \tag{10}$$

$$\frac{dM_o}{dt} = 2k_{d0}D'_o - 2(k_{a0} + k_{a1})/(\upsilon_o L){M_o}^2 + k_{on1}LM_w - k_{off1}M_o + 2k_{d1}D_o - k_{a2}/(\upsilon_o L)M_oD_o + k_{d2}T_{ins} \tag{11}$$

$$\frac{dD_o}{dt} = k_{a1}/(\upsilon_o L){M_o}^2 - k_{d1}D_o - k_{a2}/(\upsilon_o L)M_oD_o + k_{d2}T_{ins} \tag{12}$$

$$\frac{dT_{ins}}{dt} = k_{a2}/(\upsilon_o L)(M_oD_o + M_iD_i) - 2k_{d2}T_{ins} \tag{13}$$

inner leaflet species

$$\frac{dM_i}{dt} = -2k_{a1}/(\upsilon_o L){M_i}^2 + 2k_{d1}D_i - k_{a2}/(\upsilon_o L)M_iD_i + k_{d2}T_{ins} \tag{14}$$

$$\frac{dD_i}{dt} = k_{a1}/(\upsilon_o L){M_i}^2 - k_{d1}D_i - k_{a2}/(\upsilon_o L)M_iD_i + k_{d2}T_{ins} \tag{15}$$

carboxyfluorescein efflux

$$\frac{dCF_{out}}{dt} = k_{eflx}(1 - CF_{out})T_{ins}/(\upsilon_o L) \tag{16}$$

The rate of dye efflux is given by eq 16, where CF_{out} is the fraction of carboxyfluorescein outside the vesicle. This expression can be derived by applying the mass action law to the reaction between the inserted trimer and carboxyfluorescein or by using a so-called "radiation boundary condition" on the outside surface of the vesicle (*32*). We found experimentally that this relation is valid because the dye efflux profile does not depend on the initial dye concentration inside the vesicles (data not shown). All concentrations, whether referring to solution species or membrane-bound species, are expressed relative to the total aqueous solution volume, thus the need for the $\upsilon_o L$ correction factors, where $\upsilon_o \simeq 0.60/2$ is the specific molar volume of the peptide on the membrane (0.60 M^{-1}), assuming a 15 Å average peptide

width, divided by 2 to correct for the two leaflets of the lipid bilayer. For example, the concentration of bound monomer relative to the lipid is $m_o = M_o/(\upsilon_o L)$, M_o being its concentration relative to water. In each of the three types of kinetic experiments performed (equilibria in aqueous solution, solution plus vesicles, and reverse experiment), the initial concentrations were calculated from the rate constants, using the appropriate partition function (*36*). Guesses for the initial concentrations were corrected until self-consistency was achieved in each case. The sets of differential equations were solved by numerical integration with a fifth-order Runge−Kutta method with constant step size (*33*). The numerical solution was directly fitted to the experimental data with a simplex algorithm. Initial guesses for the rate constants were obtained from analytical approximations of the equations and from our previous kinetic studies of amphiphile−membrane interactions (*34*, *35*).

For the self-association of δ-lysin in water, the partition function is

$$Q_w = M_w + {M_w}^2/K_2^* + {M_w}^4/(K_1^*(K_2^*)^2) \qquad (17)$$

where $K_2^* = k_{d2}^*/k_{a2}^*$, $K_1^* = k_{d1}^*/k_{a1}^*$. The initial concentrations of the δ-lysin species are then given by $M_w = \delta_o M_w/M_t$, $D_w = \delta_o({M_w}^2/K_2^*)/M_t$, and $T_w = \delta_o {M_w}^4/(K_1^*(K_2^*)^2)/M_t$, where δ_o is the total concentration of δ-lysin at time zero after mixing in the stopped-flow system, T_w, D_w, and M_w are the concentrations of δ-lysin tetramers, dimers, and monomers in aqueous solution, and the total concentration of peptide units is $M_t = \partial \ln Q_w/\partial \ln M_w$.

The rates (k_{a1}^*, k_{a2}^*, k_{d1}^*, and k_{d2}^*) and initial conditions obtained in this fashion were then used for the complete scheme. That includes self-association in water and membrane-associated processes expressed mathematically by eqs 7−16, which were used to fit the carboxyfluorescein efflux and the U6 fluorescence curves, by adjusting the remaining rate constants. The kinetic traces from the three separate experiments (carboxyfluorescein efflux, U6 fluorescence in the outer leaflet, U6 fluorescence in both leaflets) for each concentration of POPC LUVs were first fitted simultaneously. The process was iterated several times, progressively narrowing the bounds imposed on the parameters in order to find those values that fit all curves, until a global fit was achieved, with only a small range of variation for each rate constant. In the end, each carboxyfluorescein efflux curve was fitted individually, and each pair of U6 experiments simultaneously, keeping the parameters within the narrow bounds in all cases.

For the experiments with U6 in the outer leaflet only, the kinetics of U6 fluorescence were fitted using

$$F_{U6}(t) = A_o(\gamma M_o + \sum_{Y_\nu} \nu Y_\nu) - Z_o \qquad (18)$$

and with U6 in both leaflets of the vesicles

$$F_{U6}(t) = A_o(\gamma(M_o + M_i) + \sum_{Y_\nu} \nu Y_\nu) - Z_o \qquad (19)$$

where A_o and Z_o are the amplitude and zero offset of the curves and γ is the improved transfer efficiency from the bound monomer M_o relative to all other species, which were attributed the same efficiency of transfer (adding more parameters would result only in a marginal improvement of the fit). Y_ν represents all other δ-lysin species, with ν monomers $\nu = 1, 2, \ldots$. Both membrane-bound species and solution species had to be included. This is because the on-rates are far from diffusion-limited and δ-lysin in solution will collide many times with the membrane before binding, transferring energy to the U6 probe in the process, just like a ligand collides with and bounces off the membrane before binding to its receptor (*37*), and because some U6 in solution (up to about 20%) also contributes to the signal. Equations 18 and 19 were fitted to each pair of U6 fluorescence experiments simultaneously.

For the reverse experiment described below in the Results section, an additional block of equations was added, corresponding to the initial state in the donor vesicles preequilibrated with δ-lysin. This block is similar to the block corresponding to δ-lysin association to vesicles, eqs 10−15 above. The flowchart for the reverse experiment is thus δ-lysin in donor LUVs (no dye) → δ-lysin in solution → δ-lysin in acceptor LUVs (dye loaded). The initial conditions were calculated, as described for the solution case above, from the partition function

$$Q_m = \frac{K_{D1}}{L}\left(M_o + \frac{{M_o}^2}{K_2^*(L/K_{D1})} + \frac{{M_o}^4}{K_1^*(K_2^*)^2(L/K_{D1})^3}\right) + 2\left(M_o + \frac{{M_o}^2}{K_0\upsilon_o L} + \frac{{M_o}^2}{K_1\upsilon_o L}\right) + \frac{{M_o}^3}{K_1K_2(\upsilon_o L)^2} \qquad (20)$$

where the equilibrium constants are all dissociation constants given by $K_{D1} = k_{off1}/k_{on1}$, $K_0 = k_{d0}/k_{a0}$, $K_1 = k_{d1}/k_{a1}$, $K_2 = k_{d2}/k_{a2}$, $K_2^* = k_{d2}^*/k_{a2}^*$, and $K_1^* = k_{d1}^*/k_{a1}^*$. The total δ-lysin concentration expressed in terms of peptide units per aqueous solution volume is then given by $M_t = \partial \ln Q_m/\partial \ln M_o$, and the concentration of each species is obtained by dividing each term in Q_m by M_t (*36*).

RESULTS

Kinetics of Carboxyfluorescein Efflux. The time course of carboxyfluorescein efflux is strongly sigmoidal at small lipid concentrations as shown by the effect of adding 0.5 μM δ-lysin to 25 μM POPC vesicles (LUVs) containing the dye (Figure 1A). This suggests that a series of steps are required before dye efflux occurs (*38*) or that a cooperative process is involved (*36*). The efflux rate depends strongly on lipid concentration over a range of almost 2 orders of magnitude (Figure 1A−H): efflux is fastest for the smallest lipid concentration (25 μM) and slowest for the largest lipid concentration (1200 μM), with the δ-lysin concentration kept constant (0.5 μM). This observation implies that the efflux rate increases with peptide concentration on the lipid vesicles, strongly suggesting that the assembly of a critical number of peptides on the vesicle is a mandatory step for release of entrapped carboxyfluorescein.

Kinetics of Fluorescence Energy Transfer from Trp to U6. Dye efflux is only the last step in the process of δ-lysin interaction with POPC LUVs. To propose a detailed mechanism, it is necessary to probe intermediate steps in the process, determining the location of δ-lysin in the vesicles as a function of time. Therefore, we investigated the kinetics of Förster energy transfer (*39*) from the single tryptophan

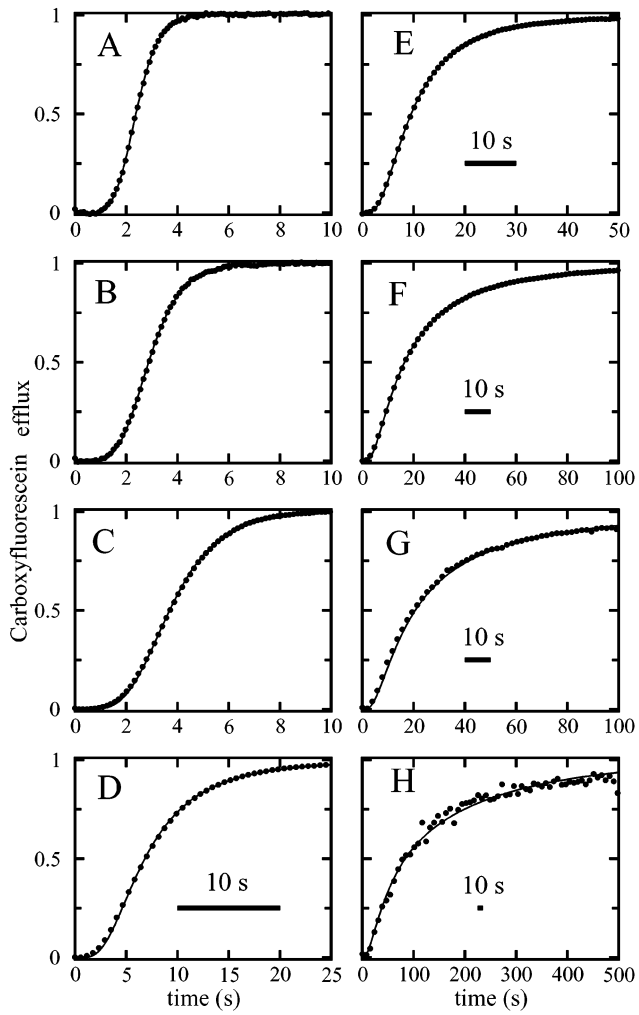

FIGURE 1: Kinetics of carboxyfluorescein efflux from POPC LUVs after δ-lysin (0.5 μM) addition. The curves correspond to (A) 25, (B) 50, (C) 100, (D) 200, (E) 300, (F) 400, (G) 600, and (H) 1200 μM lipid. The experimental traces are plotted, showing only every third to seventh point for the sake of clarity. The line is the fit of the theoretical kinetic model to the experimental data (fit parameters given in Table 1). Please note the 10 s bars, which are included to emphasize that the *X*-axis scales vary.

residue in δ-lysin (Trp15) to the U6 fluorescent probe located in the bilayer. Matsuzaki and co-workers have applied this method to the study of magainin interaction with lipid vesicles (*40*, *41*), and Wimley and White (*42*) expanded it for equilibrium topological studies of peptides in membranes. U6 is a single-chain amphiphile with a fluorescent headgroup that accepts Förster energy transfer from tryptophan, with a value of $R_o \simeq 25$ Å, similar to that for lysomethylcoumarin (*42*), a related lipid fluorophore. The U6 molecule is anchored in the bilayer by a tetradecane, saturated hydrocarbon chain, while the fluorophore proper remains above the bilayer, in the aqueous medium (*34*). Energy transfer from Trp15 to U6 is expected to be most efficient if δ-lysin is bound to the membrane with the Trp in contact with the water, not buried in the bilayer or in a peptide aggregate. Note that Trp15 is not located in the hydrophobic side of the δ-lysin amphipathic α-helix but in the hydrophilic face or in the interface between the two sides of the helix, depending on the side chain conformation. Fluorescence energy transfer efficiency is significant if the donor−acceptor distance R is close to the Förster radius R_o but decays rapidly, as $1/(1 + (R/R_o)^6)$, as the Trp in δ-lysin moves away from U6 in the membrane. The advantage of kinetic over equilibrium measurements is that transients provide additional information about nonuniform peptide distributions at certain times, even if the equilibrium distribution may be uniform.

LUVs labeled with U6 on the outer leaflet of the bilayer were prepared by adding U6 from a concentrated solution in ethanol to a suspension of preformed lipid vesicles. Association of the fluorophore with lipid vesicles is fast, with an on-rate $\simeq 2 \times 10^5$ M^{-1} s^{-1}, and with a dissociation constant $\simeq 5$ μM relative to total lipid, at room temperature (*34*, *35*). Following δ-lysin addition to the vesicles in the stopped-flow system, the time course of U6 fluorescence upon excitation of the Trp was measured. If the peptide bound to the vesicle and remained monomeric at the membrane surface, U6 fluorescence should increase until a plateau was reached. On the other hand, if binding was followed by any process that increased the average Trp−U6 distance, such as peptide self-association on the membrane surface, insertion into the bilayer, or even translocation, emission from U6 should increase initially, reach a maximum, and then decay. The latter was observed experimentally, with a clear decrease in U6 fluorescence following the initial rise (Figure 2, lower curves, U6 in the outer leaflet only).

To distinguish between the formation of a stable membrane pore and δ-lysin translocation across the membrane, a second experiment was performed where the U6 fluorophore was uniformly distributed over both membrane leaflets (U6 and POPC were codissolved in $CHCl_3$ prior to vesicle preparation). The U6 concentration in each leaflet (4 mol %) was identical to its concentration in the outer leaflet in the first experiment. If δ-lysin simply associated on the surface or inserted, forming a stable pore, the two sets should give the same result, because the U6 in the inner leaflet would not contribute to the signal; if the δ-lysin crossed the bilayer and adsorbed to the inner leaflet, the two sets of U6 fluorescence experiments should yield different results. The data shown in Figure 2 clearly indicate that the latter occurred: at high peptide concentrations per vesicle (25−100 μM lipid) the peptide translocates to the inner membrane leaflet. The total change in fluorescence after addition of δ-lysin is much smaller in the second experiment (U6 in both leaflets) because the peptide reaches the other side of the bilayer, where again energy transfer occurs; thus there is no decay in the U6 fluorescence. As the peptide density on the vesicle is lowered (by increasing the lipid concentration), the traces for both types of U6 experiments resemble each other more and more until, at 600 μM lipid, they all but merge. This observation indicates that, once the concentration of δ-lysin in the vesicles is sufficiently low, peptide insertion and crossing the membrane become a very low probability event. This is confirmed by the extremely slow dye release from carboxyfluorescein-loaded vesicles at high lipid concentration (1200 μM), shown in Figure 1H.

Two aspects need to be addressed. First, it is noticeable that in symmetrically U6-labeled vesicles, even at high lipid concentration, a decay of the energy transfer is observed (Figure 2F,G), which is not explained by peptide translocation. Second, as indicated by Wimley and White (*42*), comparison of results obtained with symmetrically and asymmetrically labeled vesicles is meaningful only when the

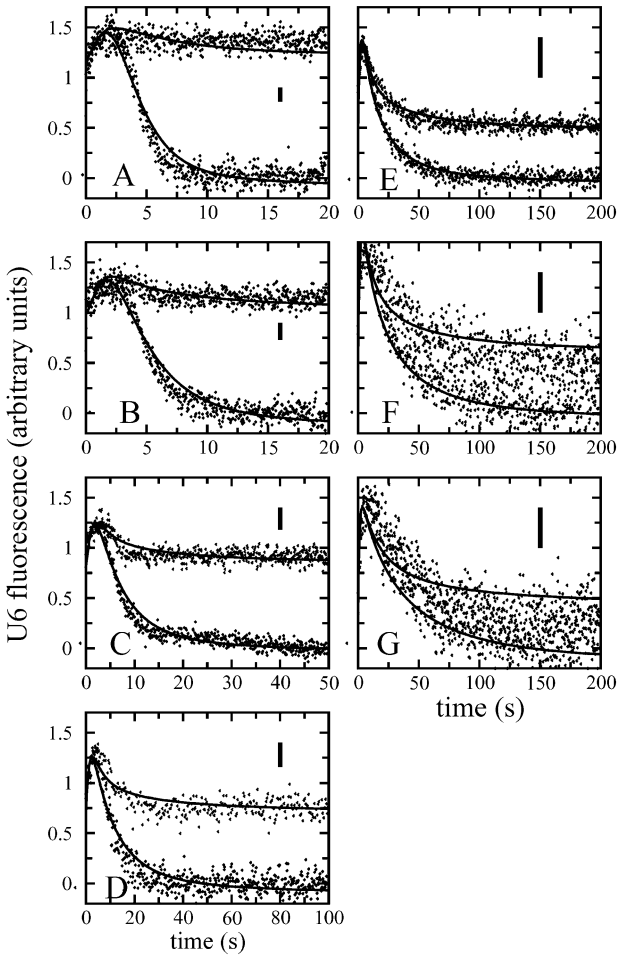

FIGURE 2: Kinetics of U6 fluorescence upon Förster energy transfer from the Trp15 of δ-lysin, following peptide addition (0.5 μM). In each panel the upper trace corresponds to U6 in both leaflets of the bilayer, and the lower trace corresponds to U6 in the outer leaflet of the bilayer only. The curves correspond to (A) 25, (B) 50, (C) 100, (D) 200, (E) 300, (F) 400, and (G) 600 μM lipid. The points are the experimental traces, which are averages of a minimum of nine shots. The smooth lines through the data are the fits of the kinetic model. The parameters are exactly the same for each pair of curves shown in each panel. The global fit parameters are given in Table 1. The scales of the U6 fluorescence are arbitrary. They are the same within each panel for both the symmetrically and asymmetrically U6 labeled vesicles, but they are different for small and large lipid concentrations [e.g., (A) 25 and (G) 600 μM POPC]. The latter are more amplified: the vertical bars represent the same signal amplitude (fluorescence counts) in all panels. In each panel, the initial point was set to 1, but with larger lipid concentrations part of the initial binding occurs in the dead time, so there is a larger uncertainty in the initial value in those cases. Likewise, the zero level is just the final level, not the absence of energy transfer. Please note that the *X*-axis scales vary.

peptide does not induce lipid flip-flop. It is clear from the discrepancy of the upper and lower traces in Figure 2A that any flip-flop induced by δ-lysin must be slow on the time scale of this experiment, 20 s. However, slow flip-flop could still occur. We will return to these two aspects after we have introduced a detailed kinetic model for δ-lysin action.

δ-Lysin Self-Association in Aqueous Solution. It is well-known that δ-lysin aggregates in aqueous solution at concentrations ≥1 μM (*15*). Because of signal intensity, it was not possible to work with concentrations much below that value; thus the δ-lysin self-association in aqueous solution had to be explicitly included in this study if a quantitative treatment was envisaged. Preliminary equilibrium measurements of Trp15 fluorescence as a function of δ-lysin concentration in aqueous solution indicated a significant change at 1 μM (data not shown), consistent with published studies. In fact, it has been proposed that δ-lysin occurs as very large aggregates at high concentrations and as tetramers above 1 μM, which dissociate into monomers below this concentration (*15*, *16*). Thus, the association of δ-lysin in solution was investigated in a separate set of experiments because the presence of aggregates in solution will influence the observed kinetics of peptide−membrane interactions. δ-Lysin solutions (in 0.1 M KCl, pH 3.0) were diluted into equal volumes of buffer in the stopped-flow apparatus to final δ-lysin concentrations of 0.25−1.0 μM. The resulting kinetics and corresponding fits are shown in Figure 3, where a simultaneous fit to the three curves is shown. We concluded that, below 1 μM δ-lysin, tetramers, dimers, and monomers are in equilibrium, according to eq 1. The molecular rate constants for self-association and dissociation, obtained from the fits of the corresponding set of differential equations to the Trp fluorescence decay curves, are included in Table 1. Those values were then used in the fits to the complete kinetics of interaction with the POPC vesicles, below.

Reversibility and Back-Reaction Rates. The molecular rate constants for the back-reactions in Figure 5 are difficult to determine from the forward reaction alone because the overall kinetics of carboxyfluorescein efflux and U6 fluorescence are not very sensitive to the backward rates, especially the off-rates from the membrane. To determine the molecular rate constants for the back-reactions and also to ensure that the process was reversible, we devised the following "reverse" reaction. In two separate experiments, POPC LUVs of different concentrations (100 and 460 μM) containing no dye were incubated with the same amount of δ-lysin (1 μM) and allowed to reach equilibrium (donors), which takes about 15 min. These suspensions were then mixed with new, carboxyfluorescein-loaded vesicles (acceptors), in such a way that the final, total lipid and peptide concentrations after mixing were the same in both cases (250 μM POPC, 0.5 μM peptide). It was expected that when the peptide/lipid ratio (P/L) in the preincubation was high (1:100), a large fraction of peptide would be in an aggregated state, whereas when the peptide was preincubated with lipid vesicles at low P/L (1:460), the equilibrium would be shifted to a monomeric state (see Figure 1A,F, where the 50 and 400 μM lipid curves have P/L values similar to the two cases now discussed). Desorption would occur more readily and, when mixed with fresh carboxyfluorescein-loaded vesicles, efflux would occur faster. Thus, if our working hypothesis was correct, the preincubation condition with P/L = 1:460 should result in faster kinetics of permeabilization of the acceptor, carboxyfluorescein-loaded vesicles than the preincubation condition with P/L = 1:100. This was indeed observed and is shown in Figure 4. The process is faster when the peptide concentration on the vesicle is smaller, as predicted. The experimental curves are also in quantitative agreement with the time course expected using the rate constants determined in the kinetic model analysis (see below), as shown by the calculated curves in Figure 4. Furthermore, this experiment showed that the association of δ-lysin with POPC is fully reversible. Light scattering at 90°

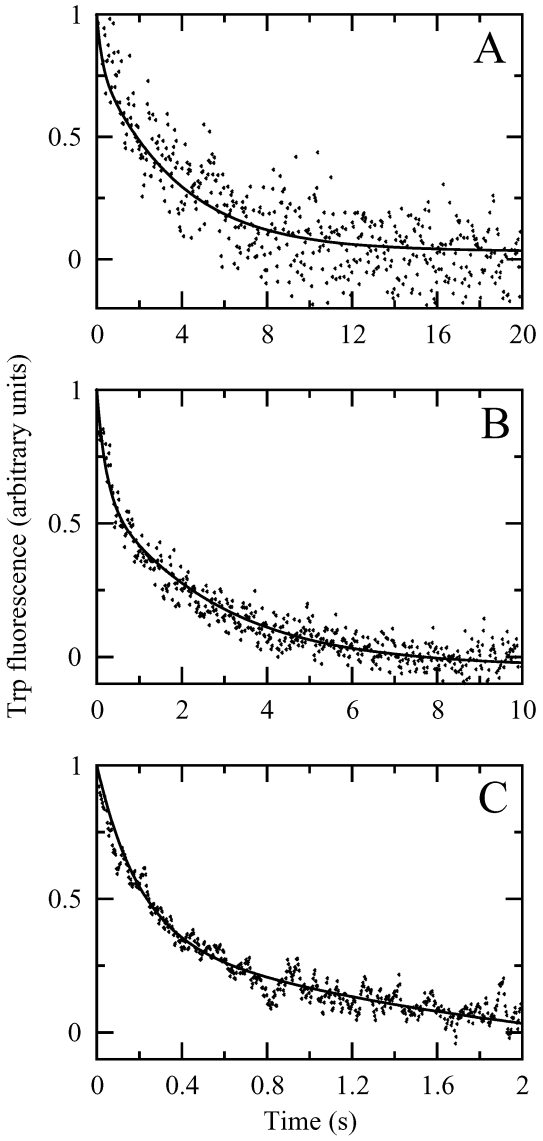

FIGURE 3: Kinetics of dissociation of δ-lysin aggregates in aqueous solution. The data points show the intrinsic fluorescence of Trp15 of δ-lysin as the aggregates dissociate upon dilution. The fluorescence units are arbitrary: the initial level was set to 1 and the final level to 0, which does not mean that the monomer fluorescence is zero. Peptide solutions of different initial concentrations were diluted into equal volumes of buffer in the stopped-flow apparatus to final δ-lysin concentrations of (A) 0.25, (B) 0.50, and (C) 1.0 μM in terms of peptide units. The lines are fits of the aqueous solution block of the kinetic model (eqs 7−9, without the membrane-related terms) to the experimental data points, shown. The fit parameters, which are listed in the left column of Table 1, are the same for the three curves shown.

showed no evidence for vesicle disintegration or formation of micellar structures upon interaction with δ-lysin.

Detailed Kinetic Model. To gain a better understanding of the mechanism of δ-lysin action upon POPC vesicles, we developed the kinetic scheme shown in Figure 5, which is expressed mathematically by eqs 1−19. It quantitatively describes the kinetics of carboxyfluorescein release and Förster energy transfer from Trp15 to U6 upon δ-lysin binding to POPC vesicles, as seen by the fits shown in Figures 1−4.

Both monomer and dimer must associate with the membrane (it is not possible to fit the kinetic traces assuming that only one or the other binds). The solution dimer D_w is

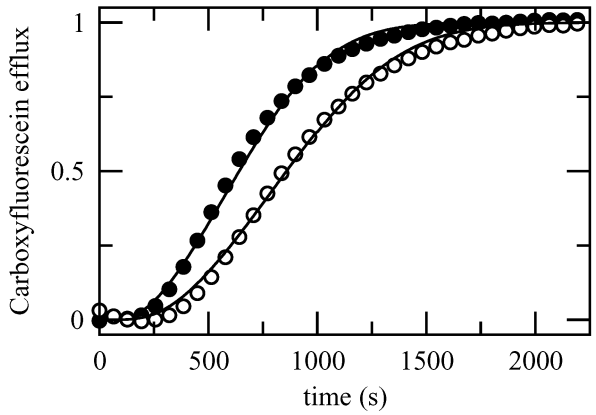

FIGURE 4: Reverse experiment for carboxyfluorescein efflux from POPC LUVs after δ-lysin addition. Please note that the time scale is much longer than in Figures 1 and 2. δ-Lysin was preequilibrated with empty vesicles (donors) in two concentrations and then mixed with carboxyfluorescein-loaded vesicles (acceptors) to the same final concentrations of lipid and peptide. The data points (only every tenth point is shown for clarity) are experimental, the line is calculated from the kinetic model using parameters ($k_{a1} = 12\ M^{-1}\ s^{-1}$, $k_{d1} = 1.2 \times 10^{-3}\ s^{-1}$, $k_{a2} = 21.6\ M^{-1}\ s^{-1}$, $k_{d2} = 0.5\ s^{-1}$, $k_{eflx} = 3.1 \times 10^{3}\ M^{-1}\ s^{-1}$) in the ranges given in Table 1. Solid symbols represent a preincubation condition with P/L = 1:460, whereas open symbols represent a preincubation condition with P/L = 1:100. Final condition is P/L = 1:500 in both cases.

probably, like the tetramer, stabilized to a large extent by hydrophobic interactions between the nonpolar faces of the amphipathic δ-lysin α-helix (*15*). After binding (D_o'), this dimer dissociates into monomers and essentially does not re-form because of competition from formation of the dimer D_o which occurs much faster. This stable, membrane-bound dimer is probably stabilized mainly by electrostatic and Trp stacking interactions (see below). A stable dimer and a monomer transiently associate to form a trimer, which translocates across the lipid bilayer and dissociates rather quickly inside the vesicle. The trimer translocation step is coupled with dye efflux.

The results shown in Figure 2 can now be fully explained. In the limit of high lipid concentration (approached in Figure 2G), the energy transfer curves are the same for symmetrically and asymmetrically U6-labeled vesicles, but a decay is still observed although translocation occurs extremely slowly. The explanation is that dimerization occurs on the vesicle surface and the efficiency of energy transfer from the δ-lysin dimer to U6 is lower than from the monomer. We discuss the reasons for the difference in energy transfer efficiency below. This is incorporated in the model, eqs 18 and 19, where γ is the ratio of energy transfer efficiency (monomer/dimer). Thus, in the limit of infinite lipid concentration, all that happens is that the peptide binds and dimerizes on the vesicle. The rise in the U6 fluorescence is due to peptide binding; the decay is due to dimerization (Figure 2F,G). The U6 fluorescence essentially follows the time course of the monomer on the outer leaflet (Figure 6B, upper dashed line). At low lipid concentration, with symmetrically U6-labeled vesicles (upper trace of Figure 2A), the energy transfer still parallels the monomer population (dashed lines in Figure 6A), but the amplitude of the decrease is much smaller. This is because the frequency of peptide−vesicle collisions is lower, and thus the amount of bound monomer is never very large, as it dimerizes rapidly on the

Table 1: Rate Constants and Equilibrium Dissociation Constants Derived from the Fits of the Model to the Experimental Data

aqueous solution		binding to vesicles		membrane	
constant	mean	constant	mean ± SD[a]	constant	mean ± SD
k^*_{a1}	$7.2 \times 10^5\ M^{-1}\ s^{-1}$	k_{on1}	$(3.6 \pm 0.2) \times 10^4\ M^{-1}\ s^{-1}$	k_{a0}	$0.32 \pm 0.06\ M^{-1}\ s^{-1}$
k^*_{d1}	$4.0\ s^{-1}$	k_{off1}	$(6.0 \pm 0.3) \times 10^{-3}\ s^{-1}$	k_{d0}	$0.8 \pm 0.1\ s^{-1}$
k^*_{a2}	$7.2 \times 10^5\ M^{-1}\ s^{-1}$	k_{on2}	$(3.9 \pm 0.1) \times 10^4\ M^{-1}\ s^{-1}$	k_{a1}	$10 \pm 2\ M^{-1}\ s^{-1}$
k^*_{d2}	$5.6 \times 10^{-2}\ s^{-1}$	k_{off2}	$(1.0 \pm 0.05) \times 10^{-2}\ s^{-1}$	k_{d1}	$(1.1 \pm 0.1) \times 10^{-3}\ s^{-1}$
				k_{a2}	$18 \pm 3\ M^{-1}\ s^{-1}$
				k_{d2}[b]	$\geq 1.1 \pm 0.5\ s^{-1}$
				k_{eflx}[b]	$(\geq 2.9 \pm 0.6) \times 10^3\ M^{-1}\ s^{-1}$
				γ	1.9 ± 0.6
$K^*_1 = k^*_{d1}/k^*_{a1}$	$5.6\ \mu M$	$K_{D1} = k_{off1}/k_{on1}$	$0.17\ \mu M$	$K_0 = k_{d0}/k_{a0}$	$2.5\ M$
$K^*_2 = k^*_{d2}/k^*_{a2}$	$0.077\ \mu M$	$K_{D2} = k_{off2}/k_{on2}$	$0.26\ \mu M$	$K_1 = k_{d1}/k_{a1}$	$0.11\ mM$
				$K_2 = k_{d2}/k_{a2}$	$\geq 61\ mM$

[a] The standard deviations express the variation of the parameters in the fits shown in Figures 1 and 2. They are not, however, the absolute uncertainties in the rate constants. Because of parameter compensation, the real uncertainties are generally much larger, and we estimate them to be about 20−50% for most parameters. [b] If k_{d2} and k_{eflx} are sufficiently large, there is a strong compensation between the two constants, and only their ratio k_{d2}/k_{eflx} can be determined. Thus, the values shown should be viewed only as lower bounds for both k_{d2} and k_{eflx}; the same applies to K_2, which is derived from k_{d2}.

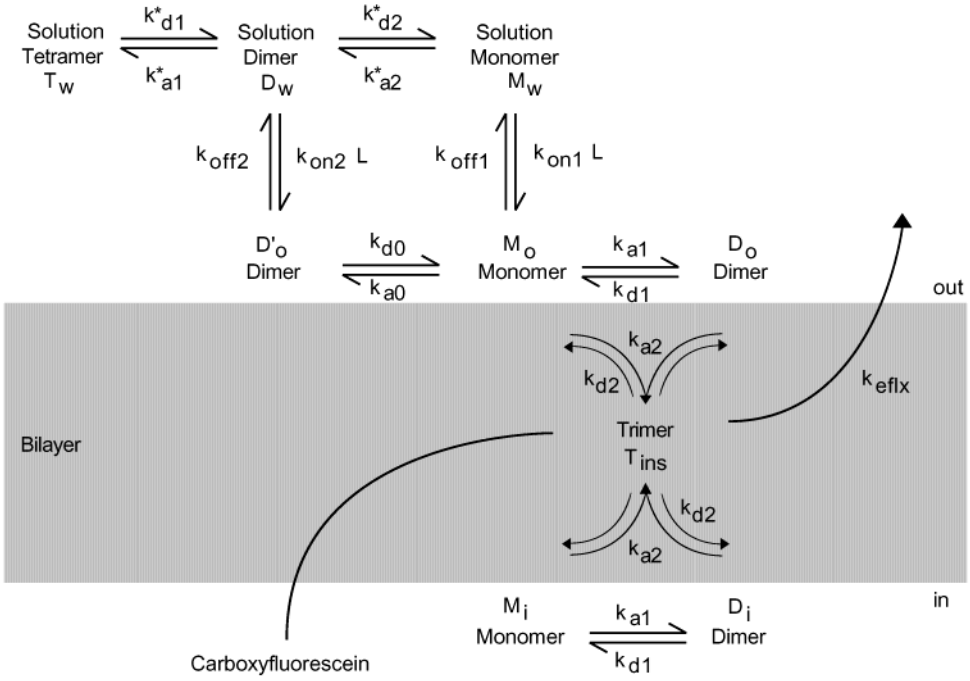

FIGURE 5: Scheme of the detailed kinetic model used to describe the experimental data for carboxyfluorescein efflux and energy transfer from Trp15 of δ-lysin to U6 in the lipid vesicles. The mathematical formulation of this model is given by eqs 7−16.

surface (low lipid). In asymmetrically labeled vesicles, energy transfer decays mainly because of translocation, which removes δ-lysin from contact with U6.

To summarize, there are two reasons for U6 fluorescence decay: (1) dimerization, which corresponds to a small change and occurs in both symmetrically and asymmetrically labeled vesicles, and (2) translocation, which corresponds to a larger change and accounts for the large decrease in U6 fluorescence at low lipid concentration in asymmetrically labeled vesicles.

The values for the best global fit of the kinetic model to the data are listed in Table 1, together with the equilibrium dissociation constants calculated from those rate constants. The constant k_{a0} for formation of the D'_o dimer was not fitted because it is determined, given all the other constants, from the thermodynamic cycle in Figure 5, $k_{a0} = k_{d0}(k_{on2}/k_{off2})(k_{off1}/k_{on1})^2(k^*_{a2}/k^*_{d2})\upsilon_o$.

The on-rates of the δ-lysin monomer and dimer onto the lipid vesicles are both similar, $\simeq 4 \times 10^4\ M^{-1}\ s^{-1}$, which is far from the diffusion limit, $\simeq 10^6\ M^{-1}\ s^{-1}$. These values are one-fifth of those obtained for some 18 amino acid amphipathic α-helical peptides, $\simeq 2 \times 10^5\ M^{-1}\ s^{-1}$ (*43*), a cyclic antimicrobial decapeptide, $1.4 \times 10^5\ M^{-1}\ s^{-1}$ (*44*), or even a single-chain lipid amphiphile, $2 \times 10^5\ M^{-1}\ s^{-1}$ (*34*), at similar temperatures. The off-rates for the δ-lysin monomer and dimer from the membrane are both $\simeq 0.01\ s^{-1}$, which is 1 order of magnitude smaller than measurements reported for the two peptides in the studies mentioned (*43*, *44*). With those values for the on- and off-rates, the equilibrium dissociation constants are both close to 0.2 μM in terms of lipid, which corresponds to $\Delta G^\circ = -9$ kcal/mol for δ-lysin (monomer or dimer) binding to a POPC LUV. This free energy change is similar to that found for magainin and some related peptides binding to POPC membranes, about −8 kcal/

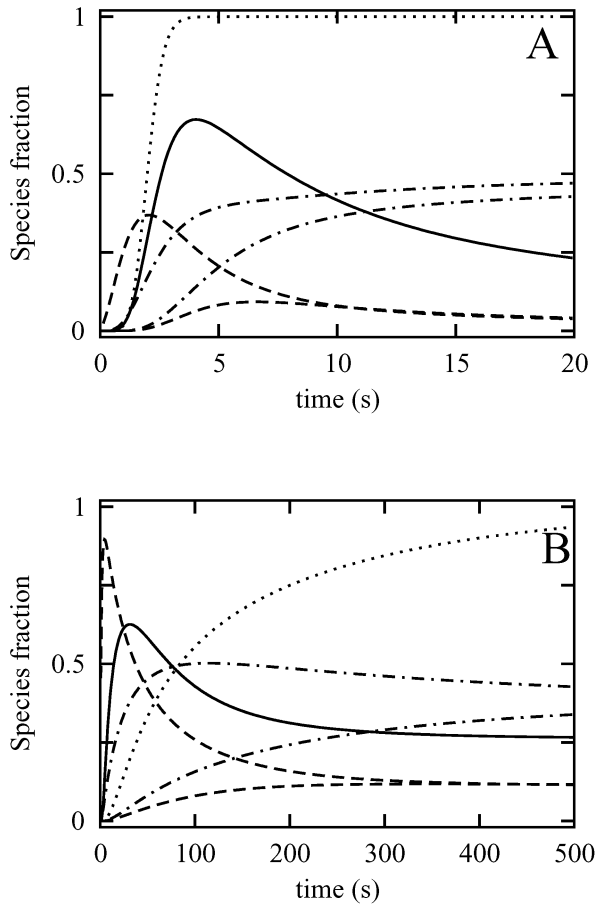

FIGURE 6: Time dependence of the populations of the various δ-lysin species calculated from the kinetic model, given as the fraction of peptide units in each form relative to the total peptide units. (A) 25 μM lipid (P/L = 1:50). (B) 1200 μM lipid (P/L = 1:2400). The δ-lysin concentration is 0.5 μM in both cases. In both panels, the dotted line is the carboxyfluorescein efflux, the solid line is the inserted trimer [$\times$30 in (A) and $\times$300 in (B)], the dashed lines are monomers on the outer and inner surface of the vesicle membrane, and the dashed−dotted lines are dimers on the outer and inner surface of the vesicle membrane. In the cases of monomers and dimers the curve that rises first represents the species on the outer leaflet, that which rises last the species on the inner leaflet. They both converge at the end of the two plots.

mol (*19*), but because mole fraction-based units were used in that study, we must add −2 kcal/mol ($-kT$ ln 55.5) to our value for purposes of comparison.

Finally, the influence of slow lipid flip-flop on our kinetic analysis can be evaluated. Two other amphipathic peptides, magainin (*45*) and mastoparan X (*46*), have been shown to induce flip-flop in phospholipid vesicles. In unperturbed vesicles, lipid flip-flop is extremely slow, but in the presence of those peptides it occurs with a time constant of the order of 5 min. To assess the effect of peptide-induced lipid flip-flop on our results, a trimer-induced lipid randomization was incorporated in our kinetic scheme. The corresponding rate was adjusted so that the randomization process would occur in the same time scale as the results published for magainin (*45*), for a P/L = 1:100, which was approximately the ratio used in those experiments. For low lipid concentrations, namely 50 μM, for which P/L = 1:100, a very slight effect is observed in the energy transfer curve for asymmetrically U6-labeled vesicles, but this effect is totally eliminated by very small changes in the rates constants, all well within the ranges of variation indicated in Table 1. At high lipid concentrations the effect is completely negligible. This is because, at high lipid, P/L is small and the peptide perturbation of the bilayer is minimal. Thus, slow lipid flip-flop, occurring at the rates documented in the literature, in the presence of amphipathic peptides, does not affect our results to any meaningful extent.

DISCUSSION

The kinetics of δ-lysin association with large lipid vesicles and the consequent release of an entrapped dye were studied by stopped-flow fluorescence. In one type of experiment, addition of δ-lysin elicited the release of carboxyfluorescein from vesicles loaded with a self-quenching dye concentration, which resulted in an increase in carboxyfluorescein fluorescence as a function of time. The kinetics of this process were markedly sigmoidal at high P/L (1:50−1:200). Release of carboxyfluorescein was fastest when small concentrations of lipid were used, becoming very slow at large lipid concentrations, for the same peptide concentration. This is exactly opposite to a normal second-order reaction between vesicles and peptides and clearly suggested that a cooperative process occurs between the membrane-bound peptides, which is crucial for membrane penetration by δ-lysin and dye release. The simplest way to account for these observations is that δ-lysin aggregation on the vesicle is a necessary step for dye release.

A second type of experiment addressed the question of whether δ-lysin inserts into the membrane forming a stable pore, probably multimeric, or simply crosses the membrane of the vesicle, thereby perturbing its structure and thus leading to carboxyfluorescein release. This was achieved by incorporating in the bilayer a fluorescent probe (U6) that is an acceptor for Förster energy transfer from Trp15, the single tryptophan residue of δ-lysin. This experiment was performed in two variants, with U6 on the outer leaflet only and with U6 in both leaflets of the bilayer. The results indicated that at large peptide concentration on the vesicles (low lipid concentration) δ-lysin inserts only transiently and crosses the membrane to the inside of the vesicle. At small peptide concentration on the vesicle (high lipid concentration) little translocation occurred: essentially, δ-lysin stays adsorbed to the outer leaflet of the bilayer, and peptide insertion occurs very slowly. The small carboxyfluorescein release observed at these high lipid concentrations results from rare translocation events. This strengthens the hypothesis that δ-lysin aggregation on the vesicle surface is an essential step for membrane penetration.

To substantiate this qualitative interpretation, the experimental data were analyzed quantitatively using a detailed kinetic model. Out of a large number of different models tested, this is the simplest that can describe the experimental results. No other model, including those postulating that peptide aggregates other than trimers (dimers, tetramers, hexamers) were involved in insertion, could fit simultaneously the two types of U6 fluorescence experiments and the carboxyfluorescein efflux experiments over the entire range of lipid concentrations. For example, a model in which the dimer itself inserts and translocates across the bilayer is able to describe the carboxyfluorescein efflux and the energy transfer to U6 data between 25 and 200 μM lipid but fails at higher lipid concentrations. This observation emphasizes the

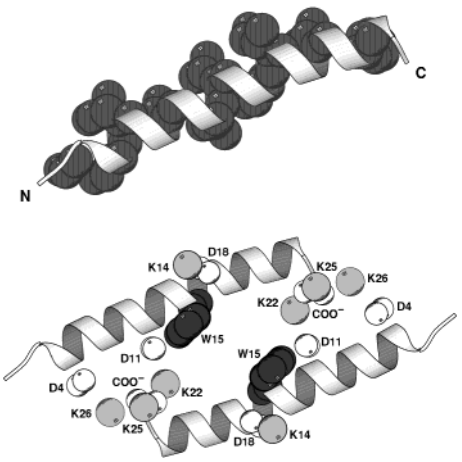

FIGURE 7: Top: Model of the δ-lysin monomer. The view shown is looking onto the hydrophilic surface. The hydrophobic residues are shown in dark. Bottom: Model of δ-lysin dimer on the membrane surface, same view as above. The charges are indicated by showing the oxygen atoms of the Asp carboxylic groups and the nitrogens of the Lys amine groups. The Trp residues are shown in dark. The monomer structure was taken from the Protein Data Bank entry 1dhl (*47*). The drawing shown here was generated with Molscript (*69*).

importance of using a very wide range of lipid concentrations when trying to estimate aggregate sizes from this type of analysis. The proposed mechanism, with constant parameters, is in good agreement with the experimental kinetic curves at all lipid concentrations, spanning almost 2 orders of magnitude.

The quantitative analysis can be summarized as follows, with reference to Figures 5 and 6. A tetramer exists in solution, which dissociates into dimers and monomers below about 1 μM peptide, as shown by other investigators (*14*, *15*) and by the present quantitative analysis of the δ-lysin dilution experiments in aqueous solution. Monomer concentration on the vesicle initially increases, following binding to the outer leaflet. The self-association of δ-lysin on the membrane surface is several orders of magnitude slower than expected for diffusion-limited aggregation. Still, a quasi-equilibrium is reached very quickly on the membrane (Figure 6), the concentration of monomers and dimers bound to the vesicle surface remaining essentially constant after an initial transient. A monomer and a dimer then associate to form a short-lived trimer, which rapidly translocates to the inside of the vesicle. Thus, the peptide surface concentration decreases on the outer leaflet of the bilayer with a concomitant decrease in the probability of trimer formation. On the inner leaflet of the membrane, a new equilibrium is established between bound monomers and dimers. At any point in time monomers and dimers constitute over 90% of the total δ-lysin population. The inserted species is always a very minor component, about 1% at 25 μM lipid and 0.1% at 1200 μM.

The stable, membrane-bound dimer is the dominant species on the vesicle (Figure 6), which is in agreement with a recent article (*16*). Careful examination of the structure of δ-lysin in an α-helical conformation (*47*) shows that two monomers lying side by side in an antiparallel orientation, with the hydrophobic faces of the helices in contact with the membrane surface, exhibit maximal interactions between the charges on the peptide (Figure 7). As pointed out by those authors (*47*), the dimer allows for two sets of intermolecular ion pairs, Asp4-Lys26 and Asp11-Lys22, in addition to two sets of intramolecular ion pairs, C-terminus-Lys25 and Asp18-Lys14. Moreover, the Trp residues are in close proximity, and stacking interactions could be involved in further stabilizing the dimer. This model also explains why the energy transfer to U6 decreases upon dimer formation: with the Trp residues on the inside of the dimer, the average distance to any U6 probe increases compared to the monomer−U6 average distance. The Gibbs free energy for dimer formation on the membrane, calculated from the rate constants k_{a1}/k_{d1}, is $\Delta G°_1 = -5.5$ kcal/mol.

In contrast, trimer formation is only very marginally favored, with $\Delta G°_2 = -1.7$ kcal/mol at most. The inserted trimer is not a stable species: it appears to be designed to avoid getting irreversibly trapped in the membrane. Its lifetime is $1/k_{d2} \leq 1$s. It is of interest to realize that it is the steady-state concentration of inserted trimer that determines the rate of carboxyfluorescein efflux, not the rate of trimer insertion (Figure 6), which does not parallel efflux. The fact that the process is reversible, as we have shown here, is consistent with translocation of δ-lysin and not with a micellization process that might occur if the peptide inserted stably into the bilayer. Matsuzaki and co-workers have argued that, in the case of the antimicrobial peptide magainin, the concentration of transient pores decreases with time, as magainin translocates into lipid vesicles (*40*, *48*). This is consistent with the mechanism proposed here for δ-lysin, which clearly indicates that the concentration of the inserted species goes through a maximum (Figure 6).

The results reported here indicate that a significant bilayer disturbance, sufficient for dye efflux and peptide translocation, can be caused by a small peptide aggregate. To try to understand this observation, we propose the following model, which is necessarily speculative because of the transient nature of the inserted trimer. In addition to the present results, a few observations are pertinent to the formulation of the model. First, the diameter of an α-helix is only slightly smaller than the thickness of the hydrophobic acyl chain region of a fluid phospholipid monolayer, about 15 Å (*49*). Second, peptide−lipid bilayer interactions depend strongly on the polar angle of an amphipathic α-helix (*50*−*52*), the angle subtended by the polar face of the helix. Third, peptides shorter than the thickness of the hydrophobic bilayer core, such as mastoparan (14 amino acids), or even shorter synthetic peptides are also able to permeabilize membranes (*53*), which is hard to reconcile with a helix orientation perpendicular to the membrane plane. Our model is represented pictorially in Figure 8, which shows the sequence of events that result in dye efflux and peptide translocation. Initially, a dimer (antiparallel) and a monomer associate. A trimer forms on the membrane surface and sinks into the outer bilayer leaflet, in a manner analogous to a "sinking raft". This is accompanied by a slight bending of the helices, sinking deeper in the middle, so that their hydrophilic terminals remain initially in contact with water. The helices then move deeper by a combination of relative rotation and downward movement. The hydrophobic residues remain in contact with the lipid acyl chains, and the hydrophilic faces of the helices line a cavity, in the center of the trimer, through which dye efflux occurs. A suggestion of the organization of the most unstable intermediate is shown in Figure 9,

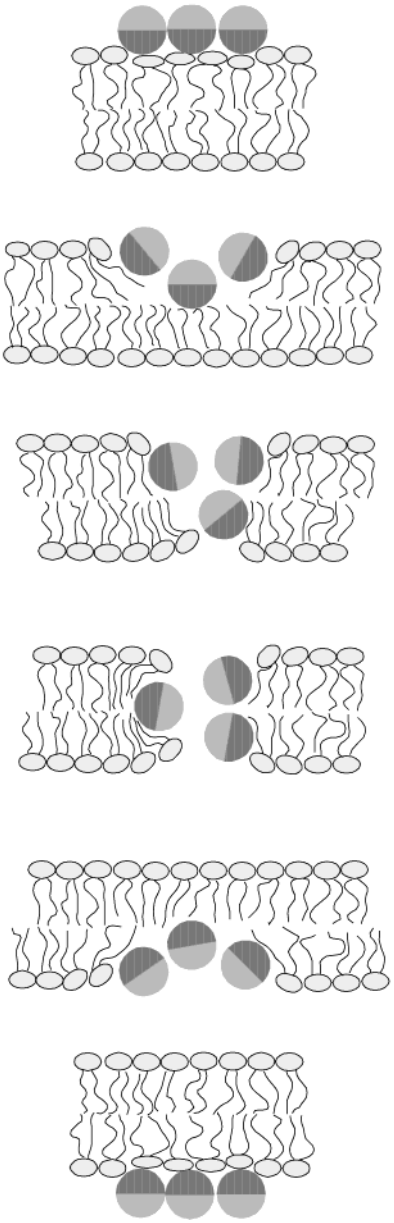

FIGURE 8: Model of the sequence of events of peptide trimer insertion and translocation across a lipid bilayer. The α-helical peptides are shown as cross sections, the darker half-circles representing the hydrophobic faces and the ligher half-circles the polar faces. The polar angle for δ-lysin is 180°. From top to bottom: Initially, a trimer forms on the surface of the phospholipid vesicle and sinks into the outer bilayer leaflet, in a manner analogous to a sinking raft. In the most unstable intermediate states (central pictures) a cavity is formed, through which dye efflux occurs. The translocation is completed in a process symmetrical to insertion and the trimer emerges on the inside of the vesicle.

corresponding to the steps in the center of Figure 8. The helices, in the bilayer, are not exactly aligned parallel, but bent in the middle. We must stress that all intermediates are presumed unstable until complete translocation occurs.

The model is proposed here for a trimer but could easily apply to other aggregate sizes, namely, dimers or tetramers. There are several additional observations consistent with this model. First, many amphipathic peptides appear to have a hinge or to be bent in the middle. The cecropins have a Gly or Pro-Gly residues close to the middle of the sequence, which in some cases breaks the helix (*54*, *55*). Buforin-2

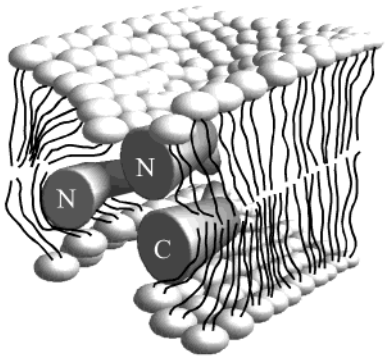

FIGURE 9: Model of the most unstable intermediate, showing a cavity lined by hydrophilic residues in the center. N or C indicate the N- and C-termini. The helices are slightly bent in the middle, approximately at the Trp15 residue, so that the lipids next to the helix termini are in contact with a hydrophobic region of the peptide.

also has a Pro residue in the middle, which appears to be essential for function (*56*). In δ-lysin, the bulky Trp at position 15 could induce a slight bend in the helix, away from the Trp, at that point. It is possible that the Phe-Gly residues in magainin function similarly. Second, for some peptides, namely, GALA (*57*), magainin-2 (*58*), and several related synthetic peptides (*51*), addition of phosphatidylethanolamine (PE) reduces peptide insertion, and addition of the peptide to PE stabilizes the bilayer structure relative to the inverted hexagonal phase. The common aspect to these observations is that peptide insertion appears to be coupled with high bilayer curvature. Third, for some peptides, namely, cecropins (*59*, *60*) and dermaseptins (*61*, *62*), the active species appears to be at most a dimer. Magainin-2 has been postulated to form a pore or to translocate across the bilayer as a large aggregate, but recently it has become apparent that a crucial role is played by a dimer, as indicated by the functional synergism with PGLa (*41*, *63*−*65*), another magainin-related peptide. How a dimer can form a pore, with the peptides perpendicular to the membrane plane, is not immediately obvious, but our model would provide a reasonable explanation. In general, the aggregate size of the translocating species might depend on the polar angle of the amphipathic helix. Smaller polar angles should favor smaller peptide aggregates, whereas larger polar angles (smaller hydrophobic faces) would require more peptides for the aggregate to be able to sink into the membrane. The synergism between different peptides may reflect an optimal combination of polar angles.

It is not easy to devise an experiment to test the existence of transient states. But if it were possible to dynamically follow the orientation of the helices relative to the bilayer plane, our sinking raft model would make a prediction that is different from most other models, namely, those postulating a pore or a torus. Unlike those models, which predict that the peptide is perpendicular to the lipid bilayer at some point, the present model predicts that the helices are always parallel to the bilayer plane.

We do not know how general this type of mechanism might be, but many other peptides that have been assumed to form stable pores might actually share it. We must point out that our experiments were performed always at relatively small P/L ratios because we believe this is the most relevant range, given the fact that these peptides are secreted into the surrounding medium and are therefore unlikely to

accumulate to very large amounts on one given target. It is possible that at much larger concentrations of peptide other forms of interaction with a membrane are preferred, which could ultimately lead to breakdown of vesicles into micelles or discoidal particles (*16*, *66*, *67*). Crossing the membrane may provide a route for the peptide to enter the cell and interact with targets located in the cytoplasm, in which case release of cell contents might not be the purpose but rather an unavoidable side effect of toxin translocation. A recent study observed no obvious correlation between the ability of a variety of antimicrobial peptides to dissipate the membrane potential in whole *E. coli* cells and their minimal inhibitory concentration (*68*). To exert their effects, however, cytolytic peptides have to interact with the plasma membrane, no matter what their final target may be. A detailed and quantitative understanding of this interaction is therefore essential.

NOTE ADDED IN PROOF

A model for the translocation and aggregation of cecropin A, which closely resembles the sinking raft model presented here, has been proposed by Silvestro and Axelsen to explain the fact that this peptide maintains an orientation parallel to the bilayer plane at all stages of its interaction with the membrane (*70*).

ACKNOWLEDGMENT

We thank Dr. Anthony Watts for a sample of synthetic δ-lysin that was used in preliminary experiments. We are also grateful to the reviewers for their useful criticism and suggestions.

REFERENCES

1. (1999) *Biochim. Biophys. Acta 1462* (an entire volume of reviews on antimicrobial peptides).
2. Saberwal, G., and Nagaraj, R. (1994) Cell-lytic antibacterial peptides that act by perturbing the barrier function of membranes: facets of their conformational features, structure−function correlations and membrane-perturbing abilities, *Biochim. Biophys. Acta 1197*, 109−131.
3. Andreu, D., and Rivas, L. (1999) Animal antimicrobial peptides: an overview, *Biopolymers 47*, 415−433.
4. Oren, Z., and Shai, Y. (1999) Mode of action of linear amphipathic α-helical antimicrobial peptides, *Biopolymers 47*, 451−463.
5. Hancock, R. E. W., and Diamond, G. (2000) The role of cationic antimicrobial peptides in innate host defenses, *Trends Microbiol. 8*, 402−410.
6. Zasloff, M. (2002) Antimicrobial peptides of multicellular organisms, *Nature 415*, 389−395.
7. Wade, D., Boman, A., Wahlin, B., Drain, C. M., Andreu, D., Boman, H. G., and Merrifield, R. B. (1990) All-D amino acid-containing channel-forming antibiotic peptides, *Proc. Natl. Acad. Sci. U.S.A. 87*, 4761−4765.
8. Nizet, V., Ohtake, T., Lauth, X., Trowbridge, J., Rudisill, J., Dorschner, R. A., Pestonjamasp, V., Piraino, J., Huttner, K., and Gallo, R. L. (2001) Innate antimicrobial peptide protects the skin from invasive bacterial infection, *Nature 414*, 454−457.
9. Blondelle, S. E., and Houghten, R. A. (1991) Hemolytic and antimicrobial activities of the twenty-four individual omission analogues of melittin, *Biochemistry 30*, 4671−4678.
10. Katsu, T., Kuroko, M., Morikawa, T., Sanchika, K., Yamanaka, H., Shinoda, S., and Fujita, Y. (1990) Interaction of wasp venom mastoparan with biomembranes, *Biochim. Biophys. Acta 1027*, 185−190.
11. Kreger, A. S., Kim, K.-S., Zaboretzky, F., and Bernheimer, A. W. (1971) Purification and properties of staphylococcal delta hemolysin, *Infect. Immun. 3*, 449−465.
12. Dhople, V. M., and Nagaraj, R. (1993) δ-toxin, unlike melittin, has only hemolytic activity and no antimicrobial activity: rationalization of this specific biological activity, *Biosci. Rep. 13*, 245−250.
13. Fitton, J. E., Dell, A., and Shaw, W. V. (1980) The amino acid sequence of the delta haemolysin of *Staphylococcus aureus*, *FEBS Lett. 115*, 209−212.
14. Fitton, J. E. (1981) Physicochemical studies on delta haemolysin, a staphylococcal cytolytic polypeptide, *FEBS Lett. 130*, 257−260.
15. Thiaudière, E., Siffert, O., Talbot, J. C., Bolard, J., Alouf, J. E., and Dufourcq, J. (1991) The amphiphilic alpha-helix concept. Consequences on the structure of staphylococcal δ-toxin in solution and bound to lipids, *Eur. J. Biochem. 195*, 203−213.
16. Talbot, J. C., Thiaudière, E., Vincent, M., Gallay, J., Siffert, O., and Dufourcq, J. (2001) Dynamics and orientation of amphipathic peptides in solution and bound to membranes: a steady-state and time-resolved fluorescence study of staphylococcal δ-toxin and its synthetic analogues, *Eur. Biophys. J. 30*, 147−161.
17. Matsuzaki, K., Nakamura, A., Murase, O., Sugishita, K., Fujii, N., and Miyajima, K. (1997) Modulation of magainin 2-lipid bilayer interactions by peptide charge, *Biochemistry 36*, 2104−2111.
18. Epand, R. M., and Vogel, H. J. (1999) Diversity of antimicrobial peptides and their mechanisms of action, *Biochim. Biophys. Acta 1462*, 11−28.
19. Wieprecht, T., Beyermann, M., and Seelig, J. (1999) Binding of antibacterial magainin peptides to electrically neutral membranes: thermodynamics and structure, *Biochemistry 38*, 10377−10387.
20. Wenk, M., and Seelig, J. (1998) Magainin 2 amide interaction with lipid membranes: calorimetric detection of peptide binding and pore formation, *Biochemistry 37*, 3909−3916.
21. Bhakoo, M., Birkbeck, T. H., and Freer, J. H. (1982) Interaction of *Staphylococcus aureus* δ-lysin with phospholipid monolayers, *Biochemistry 21*, 6879−6883.
22. Dathe, M., and Wieprecht, T. (1999) Structural features of helical antimicrobial peptides: their potential to modulate activity on model membranes and biological cells, *Biochim. Biophys. Acta 1462*, 71−87.
23. Freer, J. H., and Birkbeck, T. H. (1982) Possible Conformation of δ-lysin, a membrane-damaging peptide of *Staphylococcus aureus*, *Theor. Biol. 94*, 535−540.
24. Mellor, I. R., Thomas, D. H., and Sansom, M. S. (1988) Properties of ion channels formed by *Staphylococcus aureus* δ-toxin, *Biochim. Biophys. Acta 942*, 280−294.
25. Raghunathan, G., Seetharamulu, P., Brooks, B. R., and Guy, H. R. (1990) Models of δ-hemolysin membrane channels and crystal structures, *Proteins 8*, 213−225.
26. Kerr, I. D., Dufourcq, J., Rice, J. A., Fredkin, D. R., and Sansom, M. S. (1995) Ion channel formation by synthetic analogues of Staphylococcal δ-toxin, *Biochim. Biophys. Acta 1236*, 219−227.
27. Kerr, I. D., Doak, D. G., Sankararamakrishnan, R., Breed, J., and Sansom M. S. (1996) Molecular modelling of staphylococcal δ-toxin ion channels by restrained molecular dynamics, *Protein Eng. 9*, 161−171.
28. Bartlett, G. R. (1959) Phosphorous assay in column chromatography, *J. Biol. Chem. 234*, 466−468.
29. Birkbeck, T. H., and Freer, J. H. (1988) Purification and assay of staphylococcal δ-lysin, *Methods Enzymol. 165*, 16−22.
30. Bernheimer, A. W., and Schwarz, L. L. (1963) Isolation and composition of staphyococcal alpha-toxin, *J. Gen. Microbiol. 30*, 455−468.
31. Barreira, C. S. F. (2000) Influência do solvente na estrutura do peptideo δ-hemolisina. Relatório de Estágio, Departamento de Química, Universidade de Coimbra.
32. Crank, J. (1975) *The Mathematics of Diffusion*, 2nd ed., Oxford University Press, New York.
33. Press, W. H., Teukolsky, S. A., Vetterling, W. T., and Flannery, B. P. (1994) *Numerical Recipes in Fortran*, 2nd ed., Cambridge University Press, New York.
34. Pokorny, A., Almeida, P. F. F., Melo, E. C. C., and Vaz, W. L. C. (2000) Kinetics of amphiphile association with two-phase lipid bilayer vesicles, *Biophys. J. 78*, 267−280.
35. Pokorny, A., Almeida, P. F. F., and Vaz, W. L. C. (2001) Association of a fluorescent amphiphile with lipid bilayer vesicles in regions of solid−liquid-disordered phase coexistence, *Biophys. J. 80*, 1384−1394.

36. Wyman, J., and Gill, S. J. (1990) *Binding and Linkage. Functional chemistry of biological macromolecules*, University Science Books, Mill Valley, CA.
37. Berg, H. C., and Purcell, E. M. (1977) Physics of chemoreception, *Biophys. J. 20*, 193−219.
38. Gutfreund, H. (1995) *Kinetics for the Life Sciences*, Cambridge University Press, New York.
39. Fairclough, R. H., and Cantor, C. R. (1977) The use of singlet−singlet energy transfer to study macromolecular assemblies, *Methods Enzymol. 48*, 347−379.
40. Matsuzaki, K., Murase, O., Fujii, N., and Miyajima, K. (1995) Translocation of a channel-forming antimicrobial peptide, magainin 2, across lipid bilayers by forming a pore, *Biochemistry 34*, 6521−6526.
41. Matsuzaki, K., Mitani, Y., Akada, K. Y., Murase, O., Yoneyama, S., Zasloff, M., and Miyajima, K. (1998) Mechanism of synergism between antimicrobial peptides magainin 2 and PGLa, *Biochemistry 37*, 15144−15153.
42. Wimley, W. C., and White, S. H. (2000) Determining the membrane topology of peptides by fluorescence quenching, *Biochemistry 39*, 161−170.
43. Polozov, I. V., Polozova, A. I., Mishra, V. K., Anantharamaiah, G. M., Segrest, J. P., and Epand, R. M. (1998) Studies of kinetics and equilibrium membrane binding of class A and class L model amphipathic peptides, *Biochim. Biophys. Acta 1368*, 343−354.
44. Thomas, C. J., Gangadhar, B. P., Surolia, N., and Surolia, A. (1998) Kinetics and mechanism of the recognition of endotoxin by polymyxin B, *J. Am. Chem. Soc. 120*, 12428−12434.
45. Matsuzaki, K., Murase, O., Fujii N., and Miyajima, K. (1996) An antimicrobial peptide, magainin 2, induced rapid flip-flop of phospholipids coupled with pore formation and peptide translocation, *Biochemistry 35*, 11361−11368.
46. Matsuzaki, K., Yoneyama, S., Murase, O., and Miyajima, K. (1996) Transbilayer transport of ions and lipids coupled with mastoparan X translocation, *Biochemistry 35*, 8450−8456.
47. Raghunathan, G., Seetharamulu, P., Brooks, B. R., and Guy, H. R. (1990) Models of δ-hemolysin membrane channels and crystal structures, *Proteins: Struct., Funct., Genet. 8*, 213−225.
48. Matsuzaki, K., Murase, O., and Miyajima, K. (1995) Kinetics of pore formation by an antimicrobial peptide, magainin 2, in phospholipid bilayers, *Biochemistry 34*, 12553−12559.
49. White S. H., and Wimley, W. C. (1999) Membrane protein folding and stability: physical principles, *Annu. Rev. Biophys. Biomol. Struct. 28*, 319−365.
50. Dathe, M., Meyer, J., Beyermann, M., Maul, B., Hoischen, C., and Bienert, M. (2002) General aspects of peptide selectivity towards lipid bilayers and cell membranes studied by variation of the structural parameters of amphipathic helical model peptides, *Biochim. Biophys. Acta 1558*, 171−186.
51. Wieprecht, T., Dathe, M., Epand, R. M., Beyermann, M., Krause, E., Maloy, W. L., MacDonald, D. L., and Bienert, M. (1997) Influence of the angle subtended by the positively charged helix face on the membrane activity of amphipathic, antibacterial peptides, *Biochemistry 36*, 12869−12880.
52. Uematsu, N., and Matsuzaki, K. (2000) Polar angle as a determinant of amphipathic α-helix-lipid interactions: a model peptide study, *Biophys. J. 79*, 2075−2083.
53. Bechinger, B. (1999) The structure, dynamics and orientation of antimicrobial peptides in membranes by multidimensional solid-state NMR spectroscopy, *Biochim. Biophys. Acta 1462*, 157−183.
54. Marassi, F. M., Opella, S. J., Juvvadi, P., and Merrifield, R. B. (1999) Orientation of cecropin A helices in phospholipid bilayers determined by solid-state NMR spectroscopy, *Biophys J. 77*, 3152−3155.
55. Holak, T. A., Engstrom, A., Kraulis, P. J., Lindeberg, G., Bennich, H., Jones, T. A., Gronenborn, A. M., and Clore, G. M. (1988) The solution conformation of the antibacterial peptide cecropin A: a nuclear magnetic resonance and dynamical simulated annealing study, *Biochemistry 27*, 7620−7629.
56. Kobayashi, S., Takeshima, K., Park, C. B., Kim, S. C., and Matsuzaki, K. (2000) Interactions of the novel antimicrobial peptide buforin 2 with lipid bilayers: proline as a translocation promoting factor, *Biochemistry 39*, 8648−8654.
57. Nicol, F., Nir, S., and Szoka, F. C., Jr. (2000) Effect of phospholipid composition on an amphipathic peptide-mediated pore formation in bilayer vesicles, *Biophys J. 78*, 818−829.
58. Matsuzaki, K., Sugishita, K., Ishibe, N., Ueha, M., Nakata, S., Miyajima, K., and Epand, R. M. (1998) Relationship of membrane curvature to the formation of pores by magainin 2, *Biochemistry 37*, 11856−11863.
59. Gazit, E., Lee, W. J., Brey, P. T., and Shai, Y. (1994) Mode of action of the antibacterial cecropin B2: a spectrofluorometric study, *Biochemistry 33*, 10681−10692.
60. Gazit, E., Boman, A., Boman, H. G., and Shai, Y. (1995) Interaction of the mammalian antibacterial peptide cecropin P1 with phospholipid vesicles, *Biochemistry 34*, 11479−11488.
61. Pouny, Y., Rapaport, D., Mor, A., Nicolas, P., and Shai, Y. (1992) Interaction of antimicrobial dermaseptin and its fluorescently labeled analogues with phospholipid membranes, *Biochemistry 31*, 12416−12423.
62. Strahilevitz, J., Mor, A., Nicolas, P., and Shai, Y. (1994) Spectrum of antimicrobial activity and assembly of dermaseptin-b and its precursor form in phospholipid membranes, *Biochemistry 33*, 10951−10960.
63. Williams, R. W., Starman, R., Taylor, K. M., Gable, K., Beeler, T., Zasloff, M., and Covell, D. (1990) Raman spectroscopy of synthetic antimicrobial frog peptides magainin 2a and PGLa, *Biochemistry 29*, 4490−4496.
64. Vaz Gomes, A., de Waal, A., Berden, J. A., and Westerhoff, H. V. (1993) Electric potentiation, cooperativity, and synergism of magainin peptides in protein-free liposomes, *Biochemistry 32*, 5365−5372.
65. Westerhoff, H. V., Zasloff, M., Rosner, J. L., Hendler, R. W., De Waal, A., Vaz Gomes, A., Jongsma, P. M., Riethorst, A., and Juretic, D. (1995) Functional synergism of the magainins PGLa and magainin-2 in *Escherichia coli*, tumor cells and liposomes, *Eur. J. Biochem. 228*, 257−264.
66. Freer, J. H., Birkbeck, T. H., and Bhakoo, M. (1984) Interaction between staphylococcal δ-lysin with phospholipid monolayers and bilayers—a short review, in *Bacterial Protein Toxins* (Alouf, J., Fehrenbach, F., Freer, J. H., and Jeljasewicz, J., Eds.) pp 181−189, Academic Press, London.
67. Lohner, K., Staudegger, E., Prenner, E. J., Lewis, R. N. A. H., Kriechbaum, M., Degovics, G., and McElhaney, R. N. (1999) Effect of staphylococcal δ-lysin on the thermotropic phase behavior and vesicle morphology of dimyristoylphosphatidylcholine lipid bilayer model membranes. Differential scanning calorimetry, ^{31}P nuclear magnetic resonance, Fourier transform infrared spectroscopy, and X-ray diffraction studies, *Biochemistry 38*, 16514−16528.
68. Wu, M., Maier, E., Benz, R., and Hancock, R. E. W. (1999) Mechanism of interaction of different classes of cationic antimicrobial peptides with planar bilayers and with the cytoplasmic membrane of *Escherichia coli*, *Biochemistry 38*, 7235−7242.
69. Kraulis, P. J. (1991) MOLSCRIPT: A program to produce both detailed and schematic plots of protein structures, *J. Appl. Crystallogr. 24*, 946−950.
70. Silvestro, L., and Axelsen, P. H. (2000) *Biophys. J. 79*, 1465−1477.

BI020244R